Bioorthogonal supramolecular cell-conjugation for targeted hitchhiking drug delivery

Cheng Gao [1,†], Qian Cheng [1,†], Jianwen Wei [1,2,†], Chen Sun [1], Siyu Lu [3], Cheryl H.T. Kwong [1], Simon M.Y. Lee [1], Zhiyuan Zhong [2,*], Ruibing Wang [1,*]

[1] State Key Laboratory of Quality Research in Chinese Medicine, Institute of Chinese Medical Sciences, University of Macau, Taipa, Macao, China
[2] Biomedical Polymers Laboratory, College of Chemistry, Chemical Engineering and Materials Science and State Key Laboratory of Radiation Medicine and Protection, Soochow University, Suzhou 215123, China
[3] Green Catalysis Center, College of Chemistry, Zhengzhou University, 100 Kexue Road, Zhengzhou 450001, China

Cells possess inherent advantages to facilitate targeted payload delivery. Current strategies to conjugate payload carriers to the surface of cells are either via covalent bonds that not only involve complicated synthetic process but also often impair cellular functions, or via biological ligand-receptor interactions that are only specific to particular types of cells. Herein, we report a facile, bioorthogonal supramolecular conjugation strategy to prepare targeted cell-hitchhiking delivery systems, mediated via artificial host–guest interactions between β-cyclodextrin and adamantane, respectively anchored (via insertion) on the surfaces of live cells and payload carriers. In a paw swelling inflammation mouse model, supramolecularly conjugated macrophage-carriers (either cell–cell or cell-nanoparticle systems) were efficiently delivered hand-in-hand to the swelling paw, driven by the inflammatory tropism of macrophage. Furthermore, in an acute lung inflammation model of mouse, supramolecular conjugation of peritoneal macrophage and quercetin-loaded liposomes significantly improved targeting efficiency of the liposomes, and effectively alleviated the lung inflammation through the anti-inflammatory and anti-oxidative effects of quercetin. The cell-friendly, facile, host–guest interactions mediated cellular conjugation may provide the very first general strategy for preparing various cell-hitchhiking delivery systems to meet the needs of diverse biomedical applications.

Introduction

In order to target a specific tissue or disease site, nano-based drug delivery systems (DDSs) often rely on targeting ligands, stimuli-responsive materials or magnetic positioning [1–4]. However, these synthetic materials, either organic or inorganic, were found to be more or less immunogenic and potentially toxic [5]. A very recent study demonstrated that only 0.7% of nanoparticles decorated with trastuzumab and folic acid reached the tumor site via *i.v.* administration, and only 0.0014% penetrated into cancer cells [6]. These results revealed that most artificial DDSs were removed as "non-self" matters by the reticuloendothelial system (RES) before reaching the target tissues.

As a class of "self" component, cells have thus attracted considerable attentions as potential drug delivery vehicles due to their biocompatibility and intrinsic targeting capability to some organs and tissues [7–10], such as inflammatory tissues, or brain and bone marrow where are otherwise difficult for drugs or nanomaterials to reach[11,12]. So far, only a limited number of examples were reported to utilize live cells as drug delivery vehicles *via* either internalization of nanomaterials based drug carriers inside live cells or conjugation of drug carriers to the surface of live cells [13–15]. For drug carriers internalization inside live cells[16],

* Corresponding authors.
E-mail addresses: Zhong, Z. (zyzhong@suda.edu.cn), Wang, R. (rwang@um.edu.mo).
† These three authors contributed equally to this work.

 https://doi.org/10.1016/j.mattod.2020.05.023

they may degrade in the complexed physiological environment of the host cell, and the leaked drug may induce cellular toxicity that would negatively impact the cellular function and delivery efficiency[17–19]. For conjugation of drug carriers onto cell surface, current strategies mainly include either covalent conjugation or specific biological ligand-receptor interactions. For instance, Gu et al. constructed covalent conjugates between platelets (as carriers, decorated with anti-PD-1 antibodies) and haematopoietic stem cells (HSCs), and HSCs brought platelets to the bone marrow and locally released anti-PD-1 from platelets for anti-leukemia treatment[20]. Although improved therapeutic efficacy was observed, the covalent conjugation between HSCs and platelets involved complicated, multiple-step chemical reactions[20], which may cause impairment to the cell structure or viability, and eventually affect cell's physiological functions, including site-specific migration, and physical barriers crossing capability[21]. On the other hand, cell surface conjugation via specific ligand-receptor (e.g. antibody-antigen) interactions was only limited to specific cells that express relevant receptors, e.g. CD44, CD73 or CD90, and those interactions can be interfered in vivo due to competitive displacement[10]. Similarly, cellular "backpacks", topped with antibodies or other payload, have also been constructed via various cell surface conjugation approaches [22], including layer-by-layer assembly[23], specific ligand-receptor interactions[24], and covalent conjugation[10]. The complexity of the preparative process and/or instability of these cell surface conjugations have likely hindered clinical translation of these cellular backpacks[22]. A facile, cell-friendly, general, bioorthogonal approach of cellular conjugation for the development of live cell-based, targeted DDS has not been available so far.

On the other hand, attributed to the high biocompatibility and versatile guest-binding behaviors, β-cyclodextrin (β-CD) has been frequently utilized in molecular recognition and construction of functional biomaterials mediated via host–guest interactions [25]. Benefiting from the high binding affinity between β-CD and adamantane or its derivatives (ADA), typically between 10^4 and 10^5 M^{-1}, this supramolecular complex exhibited a good stability during systemic circulation, and therefore has often been incorporated as a noncovalent conjugation pair in drug carriers and nanomedicine for diverse biomedical applications [26,27]. 1,2-Distearoyl-sn-glycero-3-phosphorylethanolamine (DSPE) is a distearoyl (C18)-based lipid, and the alkyl chains of DSPE can be inserted into the lipid bilayer of living cells through hydrophobic interactions, resulting in anchoring the connected polymers or small molecules on cell surface [28]. For instance, DSPE-PEG has been frequently inserted into cell membrane to equip cells with PEG surface for protection of the cells against immune recognition and in vivo clearance, and for enhancing the stability of membrane modification [29]. Therefore, membrane insertion by DSPE-PEG and derivatives has become a general and widely used strategy for cell surface modification [30,31]. Herein, we report a facile strategy of bioorthogonal supramolecular cell conjugation mediated via artificial host–guest interactions, where both cell (vehicle) – liposome (hitchhiker) and cell (vehicle) – cell (hitchhiker) hitchhiking systems were constructed, as a proof of the concept, for targeted payload delivery. In particular, the supramolecular cell-liposome and cell–cell conjugates were obtained via β-CD-ADA host–guest interactions [32] between β-CD-modified vehicle cell and ADA-modified hitchhiking liposome, and between β-CD-modified vehicle cell and ADA-modified hitchhiking cell, respectively. The cell surface modification was achieved by simple ligand insertion into the cell membrane. As immune cells often exhibit inflammatory tropism to specifically accumulate in inflammatory sites [33,34], macrophage was thus selected as a live cell (vehicle) model in this study, and macrophage-liposome conjugate (MA-NP) and macrophage-L-O2 cell conjugate (MA-LO) were constructed for cell-hitchhiking payload delivery, respectively (Scheme 1). Furthermore, the improved targeting efficiency and therapeutic effects of quercetin (QT)-loaded MA-NP (namely, MA-QT-NP), when compared with those of QT-loaded liposomes, were demonstrated during the treatment of acute lung inflammation (ALI) in mouse. This approach provides the first general, cell-friendly, facile host–guest interactions mediated supramolecular cell conjugation strategy leading to cell-hitchhiking delivery systems to specifically deliver hitchhikers to the targeted sites.

Results and discussion

DSPE-PEG-β-CD and DSPE-PEG-ADA (in both cases, PEG was referred to PEG2000) were prepared and their structures were confirmed by ^{1}H NMR spectroscopy (Fig. S1). In comparison to ^{1}H NMR spectra of ADA and DSPE-PEG-NHS, DSPE-PEG-ADA featured the characteristic ^{1}H resonances of ADA at 1.64, 1.79, and 2.09 ppm, and those of DSPE at 0.85 and 1.23 ppm and that of PEG at 3.51 ppm. In comparison to ^{1}H NMR spectra of β-CD and DSPE-PEG-NHS, DSPE-PEG-β-CD featured the characteristic peaks of β-CD at 4.47, 4.82 and 5.70 ppm, those of DSPE at 0.85 and 1.23 ppm, and that of PEG at 3.51 ppm. The concentration of DSPE-PEG-β-CD and DSPE-PEG-ADA used for membrane decoration were both 10 μM, well below potentially cytotoxic concentrations (Fig. 1a) and critical micelle concentrations (CMCs) (Fig. S2).

Anchoring β-CD on macrophage surface was conveniently achieved by inserting DSPE-PEG-β-CD into the cell membrane upon co-incubation for 2 h, followed by washing and centrifuge. To demonstrate that β-CD was anchored on the cell surface and to test how long β-CD stayed on the surface, β-CD-modified macrophage was stored for 1, 4, 8 and 16 h before incubation with ADA-Fluorescein isothiocyanate (ADA-FITC) for 2 min. Strong green fluorescence was observed under confocal laser scanning microscopy (CLSM) due to the sequestration of ADA-FITC by β-CD via β-CD-ADA host–guest interactions, particularly for macrophage stored for 1 h (Fig. S3). The amplified CLSM image of β-CD-modified macrophage shown in Fig. 1b further confirmed the sequestration of ADA-FITC onto cellular surface, suggesting the presence of β-CD on macrophage surface. In contrast, nearly no fluorescence signal was detected in the control group of macrophage incubated with DSPE-PEG (Fig. 1b) and in macrophage without prior incubation with DSPE-PEG-β-CD (Fig. S3). After incubation of β-CD-modified macrophage with fresh medium for 4 or 8 h before incubation with ADA-FITC for 2 min, the green fluorescence was reduced to nearly half of that observed upon storage in fresh media for 1 h before ADA-FITC staining (Fig. S3), suggesting that only a portion of β-CD

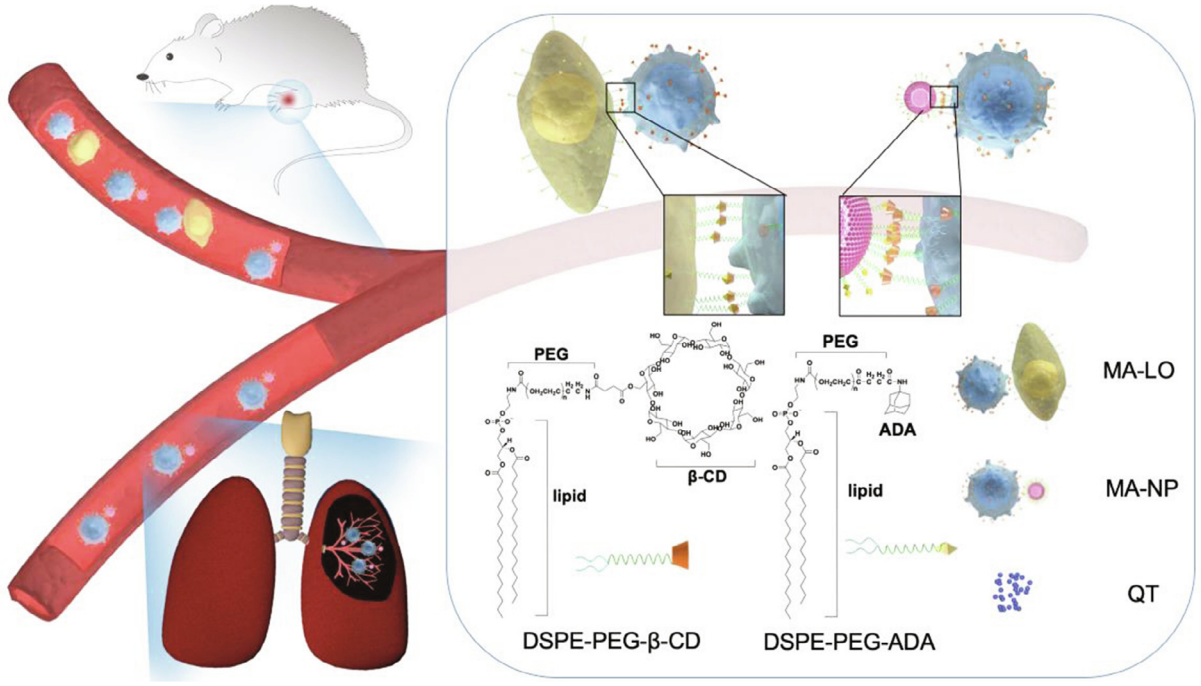

SCHEME 1

Schematic illustration of MA-NP mediated via host–guest recognition between β-CD modified macrophage (vehicle) and ADA modified liposome (hitchhiker), and MA-LO mediated via host–guest recognition between β-CD modified macrophage (vehicle) and ADA modified L-O2 (hitchhiker) for macrophage-hitchhiking delivery to the swelling paw of mouse, and targeted therapy of acute lung inflammation in mouse by MA-QT-NP.

remained on the surface after storage in the media beyond 4 h. The loss of some β-CD from the cell surface over time was likely attributed to cell membrane's fluidity and the phagocyte activity of macrophage [35]. However, the stability of β-CD surface modification for several hours is sufficient for *in vivo* cell-hitchhiking delivery due to the fast migration and targeted accumulation of cells.

Furthermore, the membrane proteins of macrophage before and after surface modification with DSPE-PEG-β-CD were analyzed via fluorescent staining of surface markers and chemokine receptors with Cy5.5-CD68 antibody, PE-F480 antibody, APC-CD11b antibody, FITC-FPR2 antibody, PE-TNFR1 antibody, and PE-TNFR 2 antibody, followed by flow cytometry analysis. The results (Fig. S4) indicated that the surface markers and chemokine receptors of macrophage before and after β-CD modification were nearly identical. Additionally, the cell migration assay of macrophage before and after surface modification (Fig. 1c) also confirmed their similar migration ability. These results suggested that surface modification with DSPE-PEG-β-CD preserved the surface properties and migration capability of macrophage.

Subsequently, ADA-modified liposome NP was constructed from DSPE-PEG-ADA, soya bean lecithin and cholesterol *via* a film dispersion method [36,37]. A spherical, stable vesicles structure was observed by transmission electronic microscope (TEM) (Fig S5). The size, size distribution and zeta potential of NPs stored over time (up to 2 months) were followed up via dynamic light scanning (DLS) analysis (Table S1), suggesting a decent stability profile. The guest-modified liposome and host-modified macrophage were subsequently co-incubated in cell culture medium without fetal bovine serum (FBS), and the scanning electron microscope (SEM) image showed that liposomes were located on cell surface (Fig. 1d). In order to further track the conjugation of liposome onto the surface of cell, doxorubicin (DOX) was loaded into ADA-modified liposome as a fluorescent tracker (DOX-NP). After incubation for 2 min, a red fluorescent layer was observed on the surface of macrophage, attributed to the bound liposomes via host–guest interactions (Fig. S6). As liposome may get internalized by macrophage over time, the intracellular uptake behavior towards DOX-NP was measured at different time intervals, initially for up to 1 h. As shown in Fig. S6 and amplified cell image in Fig. 1E, while the majority of red fluorescence from DOX-NP was still located on the surface of macrophage, a moderate level of red fluorescence was observed inside the macrophage after incubation for 1 h, indicating that most of the bound liposomes may stay on the surface of macrophage for at least 1 h. In contrast, the unmodified macrophage exhibited little fluorescence when incubated with DOX-NP under the same conditions. When incubation time with DOX-NP was increased to 4 h, more liposome was obviously internalized by macrophage (Fig. 1e), attributed to the phagocytic activity of macrophage. In fact, it only took a couple of minutes to construct macrophage-liposome (MA-NP) conjugates via quick host–guest interaction, and such conjugation was stable for at least 1 h (Fig. 1e); the system still has a significant potential for cell-hitchhiking delivery due to the fast migration and targeted accumulation of macrophage in vivo. Of a side note, an optimization study on the liposome/cell ratio suggested that a saturated binding of DOX-NPs (loading efficiency of ca. 53%) onto macrophage surface was reached with approximately 3.4 mg DOX-NPs incubated with 5×10^5 macrophage (Fig. S7).

In vivo macrophage-hitchhiking delivery of liposome was evaluated in carrageenan-induced right hind paw edema mouse

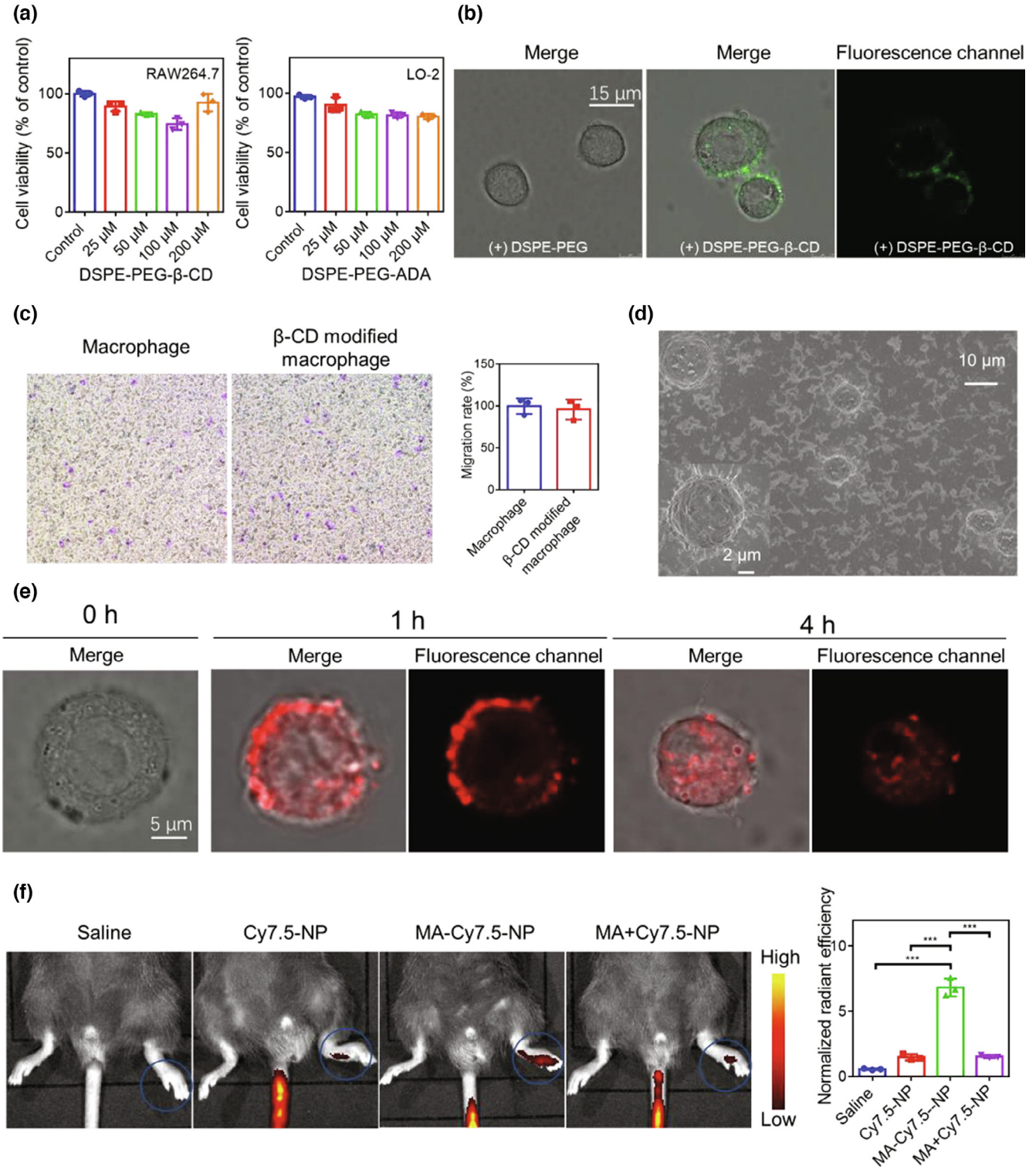

FIGURE 1

(a) Viability of RAW264.7 cells and L-O2 cells treated with DSPE-PEG-β-CD and DSPE-PEG-ADA, respectively, for 24 h at different concentrations (25, 50, 100, and 200 μM). (b) CLSM images of the physical mixture of DSPE-PEG modified macrophages and FITC-ADA (left) and DSPE-PEG-β-CD-modified macrophages and ADA-FITC (middle and right). The modified macrophages in all groups were incubated in cell culture medium without FBS for 1 h before physical mixing for CLSM imaging. (c) Cell migration analysis of macrophage before and after DSPE-PEG-β-CD modification. Macrophage were loaded on the top of transwell chamber, and DMEM containing 10 μg/L TNF-α was placed at the bottom. (d) Representative SEM image of MA-NP (inset: zoom image into a single cell). (e) β-CD-modified macrophages were incubated in cell culture medium containing DOX-NPs for different time lengths (1 and 4 h), imaged by CLSM. (f) The right paw swelling mice were i.v. administered with saline, Cy7.5-NP, MA+Cy7.5-NP, and MA-Cy7.5-NP, subsequently imaged by IVIS at 1 h post administration and quantitatively analyzed by Image Pro. All data were presented as mean ± s.d. Statistical analysis on all experiments was conducted using One-Way ANOVA. $^{*}P \leq 0.05$, $^{**}P \leq 0.01$, and $^{***}P \leq 0.001$.

model. Cyanine7.5 NHS ester (Cy7.5), a near infrared dye, was encapsulated in liposomes as a model imageable payload for *in vivo* imaging to demonstrate the potential cell-hitchhiking targeted delivery. After *i.v.* administration of Cy7.5-loaded MA-NP (MA-Cy7.5-NP), strong red fluorescence was detected in the right hind paw at 1 h post administration via *in vivo* imaging system (IVIS) (Fig. 1f), suggesting that targeted delivery of liposomes was achieved by hitchhiking macrophage. Conversely, much weaker fluorescence intensity was observed in mice treated with Cy7.5-liposomes alone (Cy7.5-NP) or physical mixture of macrophages and Cy7.5-NP (MA+Cy7.5-NP) without respective host and guest modification on their surfaces (Fig. 1f). The very modest accumulation of Cy7.5-NP in these two groups was likely attributed to passive enhanced permeability and retention (EPR) effects of nanosized liposome [38]. Collectively, these results indicated that supramolecular conjugation of macrophage and liposome enabled macrophage to carry the hitchhiker (liposomes) for targeted payload delivery to the inflammatory site of mice.

We further constructed cell–cell conjugate for potential cell-hitchhiking delivery of non-targeting cells (e.g. for potential cellular therapy), where L-O2 cell was selected as a model hitchhiker cell as it is a cell line known not to target any specific tissues. DSPE-PEG-β-CD decorated macrophage and DSPE-PEG-ADA decorated L-O2 were mixed in cell culture medium without FBS to construct the conjugate, namely MA-LO. To characterize the cell–cell conjugation, macrophages and L-O2 cells were stained by DiD (red fluorescence) (Fig. S8A) and DiO (green fluorescence) (Fig. S8B), respectively. As shown in Fig. 2a, physical mixture of macrophages and L-O2 cells without surface modification (MA+LO) did not couple with each other, and only individual cells or occasionally homo-coupled cells were observed. In contrast, hetero-cell–cell conjugation between β-CD-modified macrophages and ADA-modified L-O2 cells, MA-LO, was clearly observed (Fig. 2a). Of note, cell–cell complexes involving more than two cells were also observed, similar to the observation noted in a previously reported cell–cell conjugation system (HSCs-platelets) built via covalent bond, for targeted leukemia

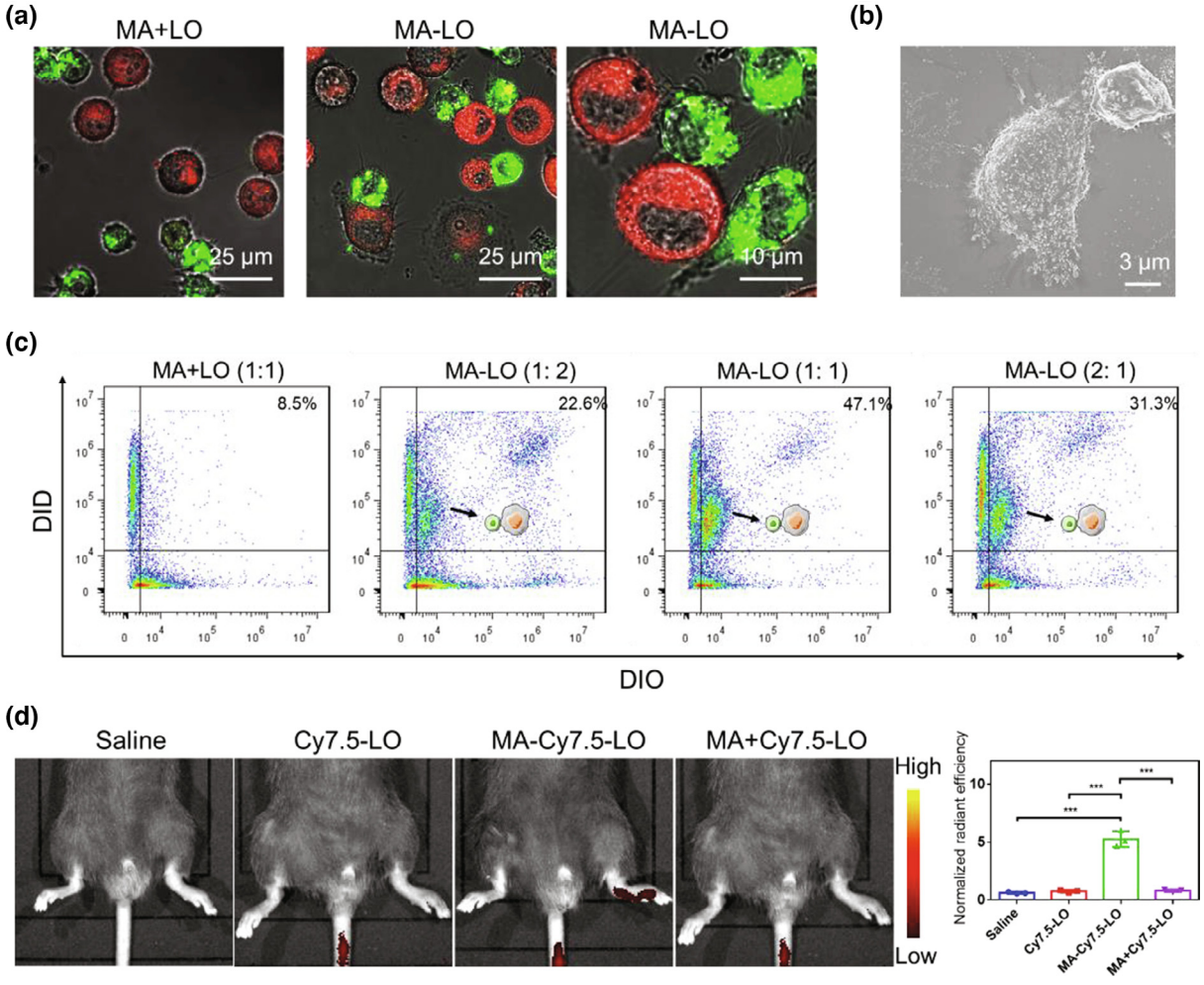

FIGURE 2

(a) CLSM images of the physical mixture of MA+LO and MA-LO conjugates, incubated in cell culture medium without FBS. Macrophage and L-O2 were stained by DiD (red) and DiO (green), respectively. (b) Representative SEM images of MA-LO conjugates. (c) The analysis of MA-LO by flow cytometry. Macrophage and L-O2 cell were mixed at the ratio of 1:1, 1:2 and 2:1 for conjugation. (d) The right paw swelling mice were administered with saline, Cy7.5-LO, MA+Cy7.5-LO (physical mixture), and MA-Cy7.5-LO, imaged by IVIS at 1 h post administration, and quantitatively analyzed by Image Pro. All data were presented as mean ± s.d. Statistical analysis on radiant efficiency was conducted using One-Way ANOVA. *$P \leq 0.05$, **$P \leq 0.01$, and ***$P \leq 0.001$.

treatment [20]. Furthermore, hetero-cell–cell (MA-LO) conjugation was confirmed by SEM (Fig. 2b). Subsequently, supramolecular cell–cell conjugation efficiency was quantitatively measured by flow cytometry. Fig. 2c showed that DiD stained the macrophages and DiO stained L-O2 cells were mainly distributed in the upper left quadrant and the bottom right quadrant of scatters, respectively, in the control group of physical mixture of both. Nearly no data cluster was found in the upper right quadrant of scatters plotting both fluorescence of DiO and DiD, indicating the separation of two types of cells. In comparison to the control group, a new data cluster was observed in the upper right quadrant of scatter by detecting both β-CD-modified macrophages and ADA-modified L-O2 cells. When the numeric ratio between macrophages and L-O2 cells was 1:1, the conjugation efficiency reached a high value of 47.1%, much higher than that achieved with other ratios such as 1:2 or 2:1 between macrophage and L-O2, as indicated by the scatter quantitation (Fig. 2c and Fig. S9 for gating strategy). Finally, the conjugates of macrophage and Cy7.5-loaded L-O2 cells, namely MA-Cy7.5-LO, were *i.v.* administered into paw swelling mice. At 1 h post administration, strong red fluorescence was observed in the inflammatory paw of mouse administered with MA-Cy7.5-LO conjugates, while nearly no fluorescence was detected in the mice treated with either Cy7.5-loaded L-O2 alone (Cy7.5-LO) or the physical mix of macrophage and Cy7.5-loaded L-O2 cells (MA+Cy7.5-LO) (Fig. 2d), suggesting that the targeted delivery of L-O2 cells to the inflammatory site was only achieved upon hitchhiking macrophages.

Finally, supramolecular cell-hitchhiking delivery system in the form of MA-NP was employed for targeted therapy in principle on ALI mouse. BALB/c mice were intratracheally administered with 50 μL of lipopolysaccharide (LPS) (1 mg/mL) for 0.5 h to induce ALI. Peritoneal macrophages in mice were isolated to prepare MA-NP conjugates. Cy7.5-loaded liposomes (Cy7.5-NP) were used for tracking the biodistribution of MA-NP conjugates. At 6 h post administration of LPS, the mice were randomly and investigator-blindly divided into three group ($n = 3$ in each group), and were subsequently *i.v.* administered with Cy7.5-NP, MA+Cy7.5-NP, and MA-Cy7.5-NP at a dose of 0.5 mg/kg Cy7.5, respectively. Due to the fast circulation in the lung [39], at 10 min post administration, all organs (including the heart, liver, lungs, spleen and kidneys) were harvested for *ex vivo* imaging. As shown in Fig. 3a and b, although majority of the dyes quickly accumulated in the liver, as was previously described for all NP-based nanomedicine, the lung of mice treated with MA-Cy7.5-NP still exhibited strongest fluorescence intensity, in comparison with those of mice treated with Cy7.5-NP and MA+Cy7.5-NP, respectively. These results again suggested that the macrophage-hitchhiking delivery system efficiently delivered attached liposomes to the inflammatory lung, due to the inflammatory tropism of the transporting macrophage.

Quercetin (QT), a dietary flavonoid found in various plants and food products, possesses anti-inflammatory and anti-oxidative properties [40]. Thus, QT was selected as the model drug, and QT-loaded liposome (QT-NP) was employed for ALI therapy. At 1 h after intratracheally administered with LPS, the mice were randomly and investigator-blindly divided into four group ($n = 6$ in each group), and were subsequently *i.v.* injected with saline, QT-NP, mixture of macrophage and QT-NP (MA +QT-NP), and macrophage-QT-NP conjugate (MA-QT-NP) at a dose of 25 mg/kg QT, respectively. Mice without LPS treatment served as the blank control group. Mice were sacrificed and the lung tissues were collected after treatment with different QT formulations for 6 h. As shown in Fig. 3c, the HE staining of the lung sections exhibited that LPS induced serious lung injuries, including infiltration of inflammatory cells into the lung interstitium and alveolar spaces, and thickening of alveolar wall. In contrast, such histological changes were markedly attenuated by treatment of all QT formulations. Among them, MA-QT-NP exhibited the best therapeutic efficacy in alleviating lung inflammation in ALI mice, as the lung tissues exhibited a clear pulmonary alveoli, similar to the blank control group. MA+QT-NP moderately alleviated the lung inflammation with a similar therapeutic efficacy to that of QT-NP. Furthermore, heme oxygenase-1 (HO-1) immunohistochemical staining showed that diverse QT formulations improved HO-1 expression in the lung tissues of ALI mice, especially in alveolar macrophages, alveolar and bronchial epithelial cells, with MA-QT-NP showing moderately better effect than the other QT formulations.

The targeted delivery of QT-NP by macrophage-hitchhiking was further confirmed by increased accumulation of MA-QT-NP in the lung tissues after treatment for 6 h (Fig. 3d), approxi -mately 2.1 fold of that in the lung tissues of mice treated with QT-NP and MA+QT-NP. To further investigate the therapeutic effects of MA-QT-NP on the lung edema of ALI mouse, the wet-to-dry ratio of the lung tissues were evaluated and analyzed, showing significantly decreased wet/dry ratio (indicative of the extent of edema) in the lung tissues of mice treated by MA-QT-NP, when compared with the rest groups (Fig. 3e). Additionally, the number of total cells and macrophages in bronchoalveolar lavage fluids (BALF) were markedly reduced in mice treated with MA-QT-NP (Fig. 3f), suggesting that MA-QT-NP dramatically ameliorated the pulmonary hyperpermeability. The release of various inflammatory cytokines plays an essential role in the pathogenesis of ALI, resulting in an increase of pulmonary permeability of the alveolar-capillary and impairment in arterial oxygenation [41]. Thus, the level of inflammatory cytokines including TNF-α and IL-1β in BALF of ALI mice were evaluated by Elisa kits. MA-QT-NP significantly decreased the lung inflammatory level (Fig. 3g), in comparison to QT-NP and MA+QT-NP. Myeloperoxidase (MPO) activity, a well-established indicator for neutrophil infiltration, was markedly attenuated in the lung tissue treated with MA-QT-NP (Fig. 3h), further confirming the effective anti-inflammation effect of MA-QT-NP. Furthermore, as an oxidative stress marker, the malondialdehyde (MDA) level in the lung was increased in ALI mice, which was also partially reversed by QT-NP, MA-QT-NP, and MA+QT-NP with similar attenuation effects (Fig. 3i), indicating the anti-oxidative activity of MA-QT-NP.

Subsequently, the lung sections in different groups of mice were also stained with Cyanine5.5 labeled F4/80 antibody and FITC labeled CD11c antibody, and Cyanine5.5 labeled F4/80 antibody and FITC labeled CD206 antibody, respectively, before analysis via CLSM. As shown in Fig. 4a, b and S10, a large number of $F4/80^{+}CD11c^{+}$ cells (M1 macrophage) and very few $F4/80^{+}CD206^{+}$ cells (M2 macrophage) were observed in the lung

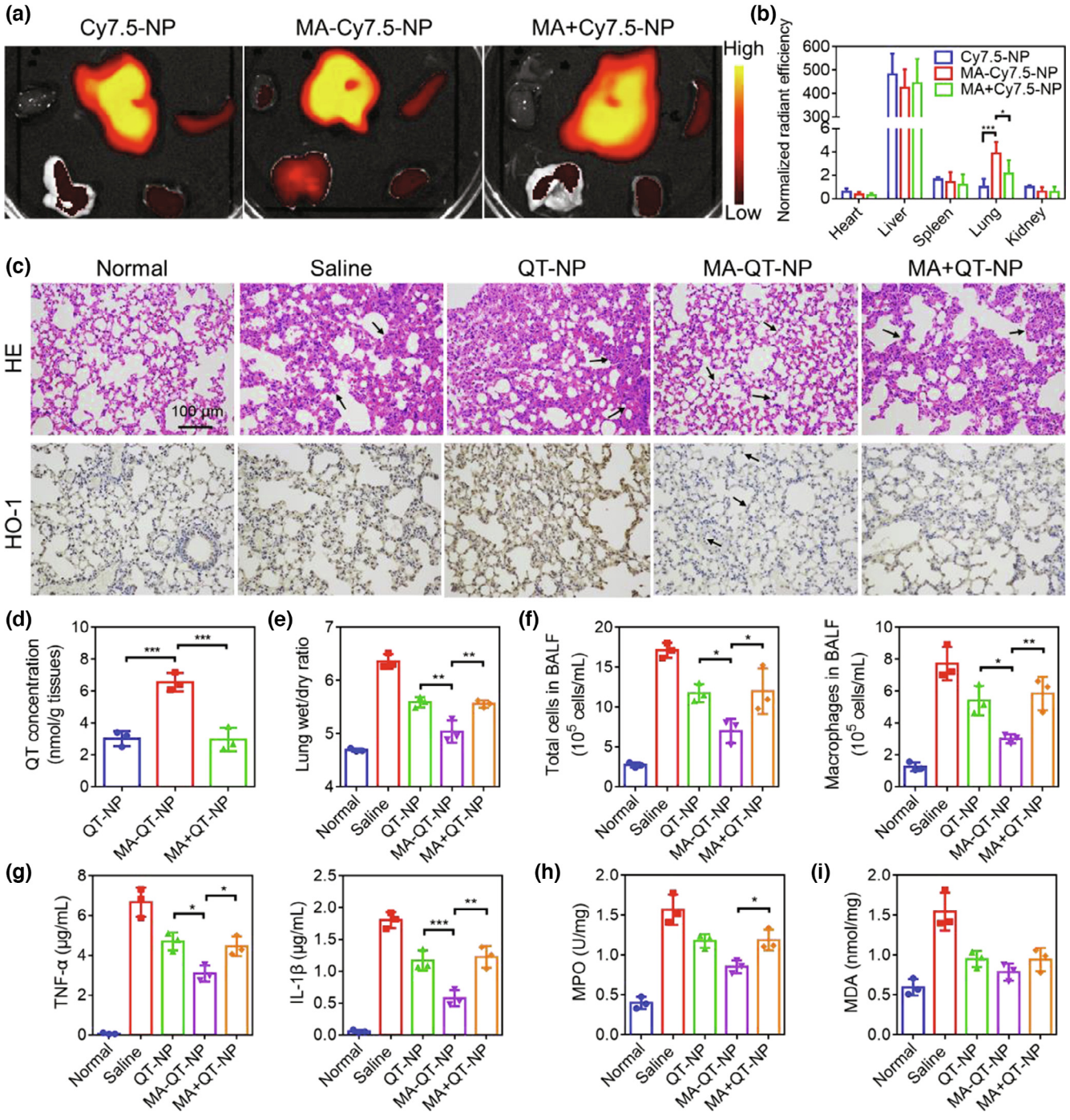

FIGURE 3

(a) Biodistribution of Cy7.5-NP, MA-Cy7.5-NP and MA+Cy7.5-NP in various organs of ALI mice via *ex vivo* imaging after treatment for 10 min. (b) Quantitative analysis fluorescence intensity in the heart, liver, spleen, lung, and kidney by in vivo image system (IVIS, Lumina XR III). (c) Histological analysis (HE staining and HO-1 staining) of the lung sections collected from ALI mice treated with Saline, QT-NP, MA-QT-NP, and MA+QT-NP at a dose of 25 mg/kg QT. Arrows in HE staining: infiltration of inflammatory cells and thickening of alveolar wall. Arrows in HO-1 staining: alveolar macrophages, alveolar and bronchial epithelial cells. Normal mice without LPS treatment served as the "normal" blank control group. (d) QT concentrations in the lung tissues collected from mice treated with QT-NP, MA-QT-NP, and MA+QT-NP, respectively. (e) Wet/dry ratio of the lungs in ALI mice with different treatments. (f) The numbers of total cells and macrophages in BALF, determined in ALI mice with different treatments. (g) TNF-α and IL-1β in BALF, detected by Elisa. (h) MPO activity and (I) MDA level in the lung tissues, measured by assay kits. All data were presented as mean ± s.d. All statistical analysis was conducted using One-Way ANOVA. $^{*}P \leq 0.05$, $^{**}P \leq 0.01$, and $^{***}P \leq 0.001$.

tissues of ALI mice treated with saline, indicating a highly inflammatory environment in the lung. MA-QT-NP effectively polarized M1 to M2 macrophage, evidenced by the significantly reduced number of $F4/80^{+}CD11c^{+}$ cells and increased $F4/80^{+}CD206^{+}$ cells, in comparison to QT-NP and MA+QT-NP. Furthermore, the homogenated lung tissues were prepared for

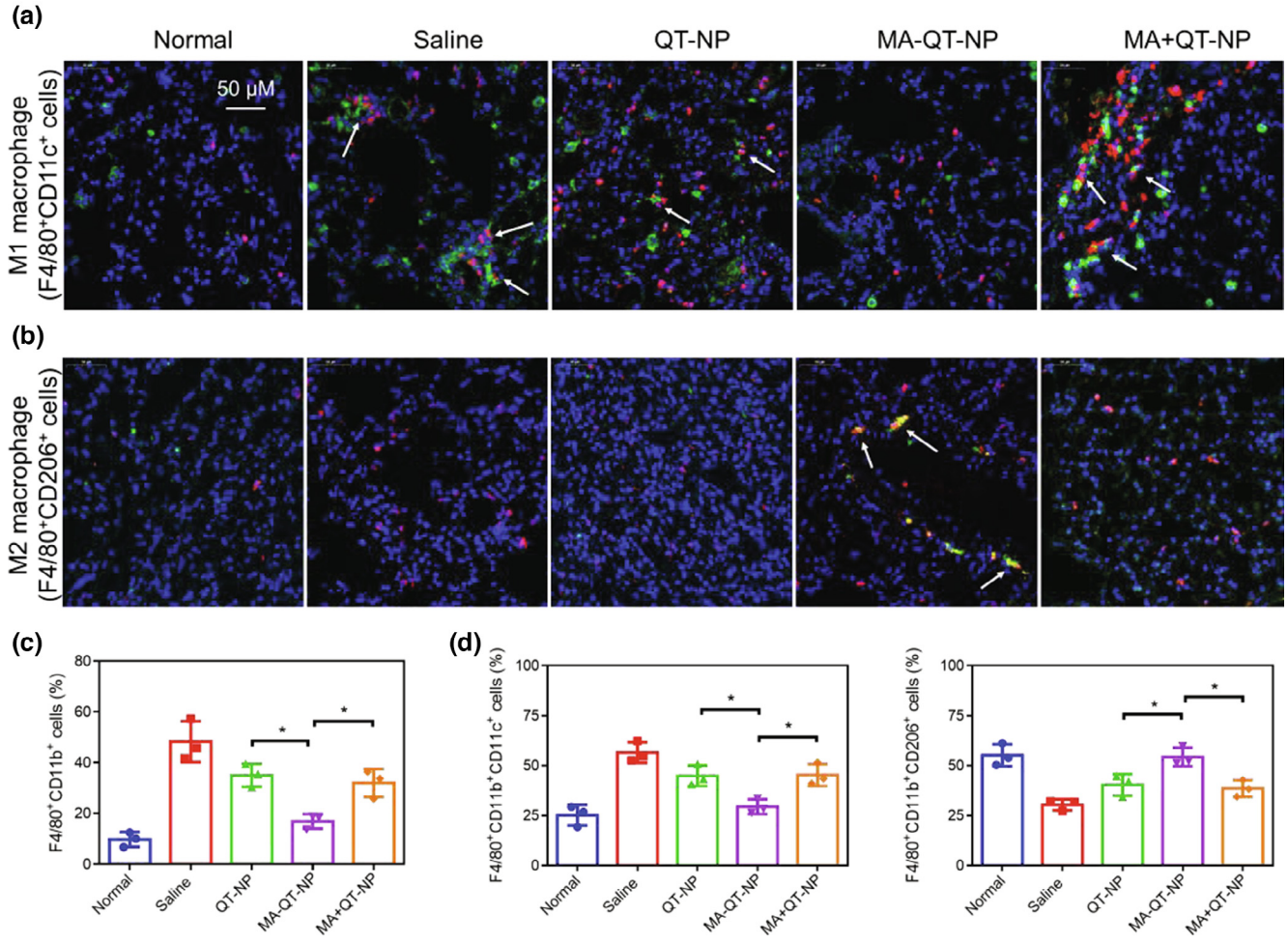

FIGURE 4

The lung sections were stained with Cyanine5.5 labeled F4/80 antibody and FITC labeled CD11c antibody (a), and Cyanine5.5 labeled F4/80 antibody and FITC labeled CD206 antibody (b). After incubation with these labeled antibodies for 1.5 h, the sections were further stained with DIPA for another 10 min, before imaging via CLSM. (c) Quantitative analysis of macrophages ($F4/80^+CD11b^+$ cells) in the lung tissues collected form ALI mice treated with Saline, QT-NP, MA-QT-NP, and MA+QT-NP, respectively; and (d) further measurement of M1 macrophage ($F4/80^+CD11b^+CD11c^+$ cells) and M2 macrophage ($F4/80^+CD11b^+$-$CD206^+$ cells) via flow cytometry.

quantitative analysis of the percentages of total macrophages ($F4/80^+CD11b^+$ cells), M1 ($F4/80^+CD11b^+CD11c^+$ cells), and M2 ($F4/80^+CD11b^+CD206^+$ cells) macrophages in the lung tissues via flow cytometry analysis. As shown in Fig. 4c and the gating strategy shown in Fig. S11, significantly lower macrophage ($F4/80^+CD11b^+$ cells) infiltration was observed in the lung tissue of MA-QT-NP treated mice in comparison to those of mice treated with QT-NP and MA+QT-NP, respectively, implying the relatively low inflammation level of the lung in MA-QT-NP treated mice. Quantitative analysis on $F4/80^+CD11b^+CD11c^+$ cells and $F4/80^+CD11b^+CD206^+$ cells further confirmed that MA-QT-NP significantly increased the M2 macrophage ratio and reduced the M1 macrophage ratio in the lung tissues (Fig. 4D), reaching the level of M1/M2 of the lung of healthy mice (the normal control group). Collectively, the results suggested that MA-QT-NP contributed to effective polarization of macrophage from M1 to M2, which, in turn, regulated and reduced the inflammatory level and alleviated ALI in mice.

Taken together, MA-QT-NP exhibited significantly improved targeting efficiency to the inflammatory lung with high drug accumulation in the lung of ALI, dramatically alleviated the lung inflammation, decreased macrophage infiltration, and polarized macrophage from M1 to M2 for inflammation regulation. In addition, the histological studies on the heart, liver, spleen, and kidneys showed no obvious toxicity of this platform, indicating an excellent safety profile of the macrophage-hitchhiking DDS (Fig. S12).

Conclusions

In summary, we developed a general, cell-friendly, facile host–guest interactions mediated bioorthogonal supramolecular cell conjugation strategy, leading to cell-hitchhiking delivery systems to specifically deliver non-targeting drug carriers to the targeted sites. Artificial receptor anchored on cell membrane may remain stable for up to at least 1 h, sufficient for *in vivo* cell-hitchhiking payload delivery. As a proof-of-principle, both nanomaterials (liposomes) and cells (L-O2) were employed as model non-targeting carriers to construct macrophage-hitchhiking conjugates, macrophage-liposome and macrophage-L-O2, respectively

prepared via this approach. Attributed to the inflammatory tropism of macrophage, macrophage-hitchhiking delivery of cells (L-O2) and nanocarriers (liposome) to the inflammatory site was demonstrated *in vivo* with a paw edema mouse model. In addition, the supramolecular cell-hitchhiking delivery system based on macrophage-liposome (loaded with quercetin) exhibited significantly improved targeting efficiency to the inflammatory lung and effectively alleviated the lung inflammation in acute lung inflammation mouse, in comparison to quercetin-loaded liposomes and the physical mixture of macrophage and quercetin-loaded liposomes. This cell-hitchhiking delivery system, mediated via host–guest interactions, is distinctively different from the live-cell based delivery system prepared via direct internalization of nanomaterial-based drug carriers inside live cell [42,43], where the internalized nanomaterial may degrade in the complex cellular environment, and the leaked drug could affect the physiological function of cells. Our macrophage-liposome conjugation process only takes a couple of minutes and the inflammatory tropism-based targeting delivery is also very quick (less than 1 h, as shown in both in vivo inflammatory models), leading to very limited intracellular uptake of liposome during conjugate preparation and payload delivery. If other cells, such as erythrocytes, are employed as the live cell carrier, instead of macrophage that is well known for high phagocytic activity, negligible intracellular uptake of the conjugated nanomedicine would be expected. In addition, surface modification with adamantane can be technically realized with any nanomedicine, for instance, via covalent functionalization. Therefore, this bioorthogonal supramolecular cell-hitchhiking strategy can be extended to a variety of other live cell-based drug delivery systems to meet the needs of diverse biomedical applications.

Author contributions

This project was conceptually designed by CG, ZZ and RW. The majority of the experiment was conducted by CG, QC and JW, assisted by SC and CK. Data analysis was conducted by CG, SL, SML, ZZ and RW. The manuscript was prepared by CG and RW. All authors discussed the results and commented on the manuscript.

CRediT authorship contribution statement

Cheng Gao: Conceptualization, Investigation, Data curation, Writing - original draft. **Qian Cheng:** Investigation. **Jianwen Wei:** Investigation. **Chen Sun:** Investigation. **Siyu Lu:** Data curation. **Cheryl H.T. Kwong:** Investigation. **Simon M.Y. Lee:** Data curation. **Zhiyuan Zhong:** Conceptualization, Data curation. **Ruibing Wang:** Conceptualization, Data curation, Writing - review & editing, Supervision.

Declaration of Competing Interest

R.W., C.G., Q.C. and S.M.Y.L. are currently applying for a patent relating to the contents of this manuscript. The remaining authors declare no competing interests.

Acknowledgements

The Science and Technology Development Fund (FDCT), Macau SAR (File No.: 0121/2018/A3, 0007/2020/A, and 0080/2020/A2) and the National Natural Science Foundation of China (Grant No.: 21871301) are gratefully acknowledged for providing financial support to this work. The authors are also grateful to Dr. Jia Chen Miss Qiaoxian Huang, Miss Ludan Yue and Mr. Tianlei Sun from University of Macau for their technical support on some of the experiments conducted during the COVID-19 pandemic.

Data availability statement

The raw data required to reproduce these findings can be provided upon request.

Appendix A. Supplementary data

Supplementary data to this article can be found online at https://doi.org/10.1016/j.mattod.2020.05.023.

References

[1] K. Ulbrich et al., Chem. Rev. 116 (9) (2016) 5338.
[2] W. Cui et al., Adv. Mater. 28 (6) (2016) 1302.
[3] W.-H. Chen et al., Adv. Mater. 31 (3) (2019) 1802725.
[4] R. Mo, Z. Gu, Mater. Today 19 (5) (2016) 274.
[5] J.J. Giner-Casares et al., Mater. Today 19 (1) (2016) 19.
[6] Q. Dai et al., ACS Nano 12 (8) (2018) 8423.
[7] A.C. Anselmo, S. Mitragotri, J. Control. Release 190 (2014) 531.
[8] R.H. Fang et al., Nano Lett. 14 (4) (2014) 2181.
[9] C.-M.J. Hu et al., Nature 526 (2015) 118.
[10] M. Ayer, H.-A. Klok, J. Control. Release 259 (2017) 92.
[11] J. Shao et al., Angew. Chem. Int. Ed. 56 (42) (2017) 12935.
[12] Y. Su et al., ACS Biomater. Sci. Eng. 1 (4) (2015) 201.
[13] M. Hamidi et al., J. Control. Release 118 (2) (2007) 145.
[14] C.-M.J. Hu et al., Adv. Healthcare Mater. 1 (5) (2012) 537.
[15] D.W. Stuckey, K. Shah, Nat. Rev. Cancer 14 (2014) 683.
[16] J. Xue et al., Nat. Nanotechnol. 12 (2017) 692.
[17] P. Foroozandeh, A.A. Aziz, Nanoscale Res. Lett. 13 (1) (2018) 339.
[18] S. Zhang et al., ACS Nano 9 (9) (2015) 8655.
[19] S. Behzadi et al., Chem. Soc. Rev. 46 (14) (2017) 4218.
[20] Q. Hu et al., Nat. Biomed. Eng. 2 (11) (2018) 831.
[21] H. Wang et al., Nat. Chem. Biol. 13 (2017) 415.
[22] N. Doshi et al., Adv. Mater. 23 (12) (2011) H105.
[23] R. Polak et al., Adv. Healthcare Mater. 4 (18) (2015) 2832.
[24] N.L. Klyachko et al., Biomaterials 140 (2017) 79.
[25] S. Gnaim et al., Chem. Sci. 10 (10) (2019) 2945.
[26] Y.M. Zhang et al., Angew. Chem. 130 (28) (2018) 8785.
[27] Y. Kang et al., Adv. Funct. Mater. 26 (48) (2016) 8920.
[28] T. Yamamoto et al., Sci. Technol. Adv. Mater. 17 (1) (2016) 677.
[29] G. Shi et al., Adv. Healthcare Mater. 3 (1) (2014) 142.
[30] N. Ding et al., Nat. Commun. 10 (1) (2019) 1336.
[31] P. Shi et al., Mater. Today 20 (1) (2017) 16.
[32] Y. Liu et al., J. Am. Chem. Soc. 130 (31) (2008) 10431.
[33] M.S. Suthar et al., PLoS Pathog. 9 (2) (2013) e1003168.
[34] C.H. Kim et al., Trends Immunol. 37 (1) (2016) 68.
[35] R. Mercier et al., Cell Reports 1 (5) (2012) 417.
[36] C. Xu et al., Nat. Commun. 9 (1) (2018) 4092.
[37] X. Sun et al., Theranostics 7 (2) (2017) 319.
[38] Y.-R. Zhang et al., Wiley Interdiscip. Rev. Nanomed. Nanobiotechnol. 11 (1) (2019) e1519.
[39] J. Guo et al., Adv. Mater. 31 (46) (2019) 1904607.
[40] G.D. Piovezana Bossolani et al., Life Sci. 238 (2019) 116956.
[41] H. Akbarshahi et al., Respir. Med. 106 (9) (2012) 1199.
[42] J. Xue et al., Nat. Nanotechnol. 12 (7) (2017) 692.
[43] W. Zhang et al., Adv. Mater. 30 (50) (2018) 1805557.